

# Encapsulation of Porphyrin-Fe/Cu Complexes into Coordination Space for Enhanced Selective Oxidative Dehydrogenation of Aromatic Hydrazides

Dongxu Zhang, Peiyao Du, Jia Liu, Ruizhong Zhang, Zhen Zhang, Zhengang Han, Jing Chen, and Xiaoquan Lu\*

The encapsulation of specific nanoentities into hollow nanomaterials derived from metal organic frameworks has attracted continuous and growing research attentions owing to their unique structural properties and unusual synergistic functions. Herein, using the phase transformation of uniform rhombi dodecahedron ZIF-67, hollow nano-shell with a well-defined morphology is successfully prepared. Particularly, the iron-oxygen complex, that is formed by the interaction between TCPP-Fe/Cu (TCPP = tetrakis(4-carboxyphenyl)-porphyrin) and oxygen, can be acted as an ideal proton acceptor for practical organic reactions. Considering the unique adaptability of hollow ZIFs (named HZ) to the transformation of encapsulated TCPP-Fe/Cu bimetallic catalytic active sites, a heterogeneous catalyst (defined as HZ@TCPP-Fe/Cu) through morphology-controlled thermal transformation and rear assemble processes is designed and constructed. Under heterogeneous conditions, HZ@TCPP-Fe/Cu serves as a multifunctional molecular selector to promote the oxidative dehydrogenation of different aromatic hydrazide derivatives with high selectivity toward primary carbon among primary, secondary, and tertiary carbons that are unachievable by other traditional homogeneous catalysts. The high catalytic activity, selectivity, and recyclability of the catalyst proposed here are attractive advantages for an alternative route to the environmentally benign transformation of aromatic hydrazides to aromatic azobenzene.

## 1. Introduction

Encapsulation of hollow nanomaterials has proven to be an effective strategy to make full use of active catalytic components and achieve a higher specific reactivity for catalyzing

heterogeneous reactions.<sup>[1–3]</sup> Distinctively, compared with other solid types of nanomaterials, thin permeable shells and limited internal voids endow the hollow nanomaterials with abundant accessible catalytic active sites and approachable contact space between specific reactants and catalysts, thus achieving efficient mass diffusion and reaction.<sup>[4–8]</sup> To tackle the problems of catalyst efficiency and selectivity, it is necessary to precisely control the positions of the different functions and spatial structures of the catalysts, but this is still a huge challenge.

Constructing multifunctional hollow nanostructured materials from multiple components is considered to be one of the promising strategies to implement high-level applications requiring complex architecture with excellent catalytic performance.<sup>[9]</sup> As previously reported, a wide range of materials could be used as “host,” such as holey Fe&N codoped graphene,<sup>[10]</sup> hollow mesoporous prussian blue nanoparticles,<sup>[11]</sup> carbon-based nanocages,<sup>[12]</sup> and layered double hydroxide

nanocages.<sup>[13]</sup> To be more specific, layered void on the cage walls can support each other for enhanced mechanical stability, thus regulating the mass transport and enhancing the contact between the active catalytic components and reactant, which could significantly improve the catalytic performances. Accordingly, the encapsulation of nanoentities in hollow layered hydroxides materials is preferred since the properties and accessibility of catalytic active sites are fit with those of heterogeneous catalysts with ideal catalytic activity and size selectivity, showing a great potential in catalysis. Thus, we aim at rationally designing a hollow nanocage that could effectively use the layered hydroxide platform to achieve effective encapsulation of catalytically active sites.

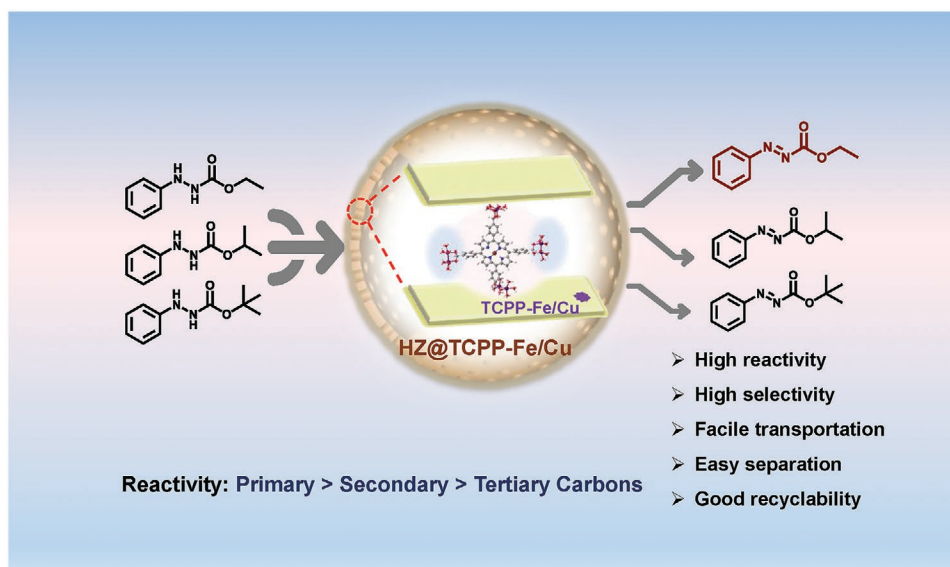
Nanoentities with specific activity as “guest,” such as single atom/site, molecule, metal nanoparticles, metal-complex, etc., are encapsulated in the limited space of “host,” so that their activity can be effectively guaranteed and thus show excellent performance.<sup>[14,15]</sup> Simultaneously, the physical and chemical properties of the “guest” are very critical factors. For instance, metalloporphyrin compounds have been extensively studied because of their rigidly and planar geometry, high thermal, and

D. Zhang, Dr. P. Du, Dr. J. Liu, Dr. R. Zhang, Dr. Z. Zhang  
Tianjin Key Laboratory of Molecular Optoelectronic Science  
Department of Chemistry  
School of Science  
Tianjin University  
Tianjin 300072, P. R. China

Dr. P. Du, Dr. Z. Han, Dr. J. Chen, Prof. X. Lu  
Key Laboratory of Bioelectrochemistry and Environmental Analysis  
of Gansu Province  
College of Chemistry and Chemical Engineering  
Northwest Normal University  
Lanzhou 730070, P. R. China  
E-mail: luxq@nwnu.edu.cn

 The ORCID identification number(s) for the author(s) of this article can be found under <https://doi.org/10.1002/sml.202004679>.

DOI: 10.1002/sml.202004679



**Scheme 1.** Schematic diagram of HZ@TCPP-Fe/Cu (where TCPP is tetrakis(4-carboxyphenyl)-porphyrin) heterogeneous catalyst applied for selective oxidative dehydrogenation of aromatic hydrazides to aromatic azobenzenes.

electronic stability.<sup>[16]</sup> And, they are also excellent candidates for interfacial charge transfer mediators in different systems.<sup>[17,18]</sup> Inspired by biomimetic catalysis, metalloporphyrin can activate oxygen under mild conditions, which is incomparable with some traditional metal salt catalysts.<sup>[19–21]</sup> In general, metalloporphyrin in organisms need to cooperate with some biological enzymes to display an excellent catalytic performance, but once isolated from these environments, the catalytic activity of individual metalloporphyrin will be greatly reduced. To solve this problem, regulating the coordination mode and microenvironment of metalloporphyrin can be an effective strategy. To be specific, an encapsulation strategy of “front introduction and rear assembly” was proposed, which successfully overcame the problem of metalloporphyrin inactivation.

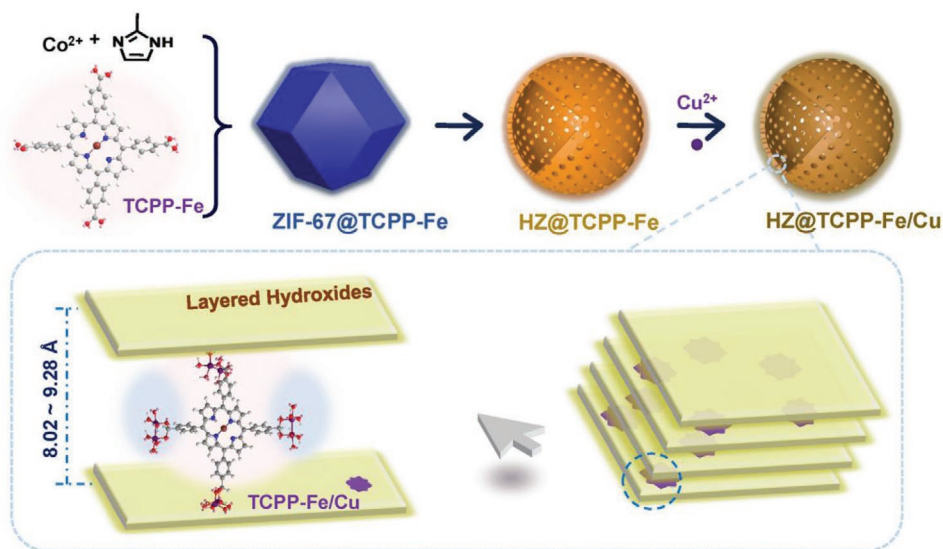
Given the unique adaptability of self-templated zeolitic imidazolate frameworks (ZIFs) in conversion of hollow ZIFs (named HZ) encapsulating TCPP-Fe/Cu (TCPP = tetrakis(4-carboxyphenyl)-porphyrin) bimetallic catalytic active sites, heterogeneous catalyst (defined as HZ@TCPP-Fe/Cu) within an integral framework was designed and synthesized. Based on the synergistic effect of TCPP-Fe/Cu bimetallic active sites and the limited internal voids oxidative dehydrogenation of aromatic hydrazides reaction was successfully obtained (**Scheme 1**). With the appropriate integration of these encapsulation strategies in the heterogeneous catalysts construction, the as-prepared hollow nanomaterials are demonstrated to be the brilliant candidates for the rational catalyst design toward the target reactions, especially for complicated industrial catalysis systems.

## 2. Results and Discussion

A self-templated strategy to construct hydrangea-like superstructure of hollow nanocatalyst through morphology-controlled thermal transformation of porous ZIFs and postassembly of bimetallic catalytic active sites were presented. To be specific,

TCPP-Fe was encapsulated into the nanocrystals of ZIF-67 *in situ* via the “bottle around ship” (named ZIF-67@TCPP-Fe). Subsequently, by treating the ZIF-67@TCPP-Fe with  $\text{Co}^{2+}$  at 120 °C for 1 h, the polyhedral would ready vanish and form hollow layered hydroxides nanocage with beneficial channel size and well-defined morphology (named HZ@TCPP-Fe). Then, the above hollow nanomaterial served as an ideal porous support and TCPP-Fe as a felicitous  $\text{Cu}^{2+}$  supplier for TCPP-Fe/Cu bimetallic catalytic active sites inside the layered hydroxides voids with excellent dispersity, and the HZ@TCPP-Fe/Cu heterogeneous catalyst was finally fabricated (**Scheme 2**).

Scanning electron microscopy (SEM) images of as-obtained ZIF-67, ZIF-67@TCPP-Fe, HZ@TCPP-Fe, and HZ@TCPP-Fe/Cu were shown in **Figure 1**. The SEM image of ZIF-67 displayed a uniform rhombi dodecahedron structure with average crystal size of about 2  $\mu\text{m}$  (Figure 1a). And the SEM image demonstrated that the overall morphology of the as-prepared ZIF-67@TCPP-Fe had not changed significantly, while the average size was reduced to  $\approx 800$  nm (Figure 1b). Besides, HZ@TCPP-Fe and HZ@TCPP-Fe/Cu displayed hydrangea-like morphology with an average diameter of  $\approx 800$  nm, and hollow nanocage had a thickness of  $\approx 20$  nm (Figure 1c–f). The as-prepared HZ@TCPP-Fe/Cu heterogeneous catalyst presents a relatively uniform size (Figure S1, Supporting Information). The dark-field scanning transmission electron microscopy (dark-field STEM) and the elemental mapping images of HZ@TCPP-Fe and HZ@TCPP-Fe/Cu confirmed that Fe and Cu elements were homogeneously dispersed (Figure 1g–r). The results of inductively coupled plasma optical emission spectrum (ICP-OES) showed that Fe and Cu were successfully doped (Table S1, Supporting Information). The synthesis routes and the details of TCPP-Fe and  $\text{H}_4\text{TPP-Fe}$  were described in the Supporting Information (Figures S2–S8, Supporting Information). To further gain insight into the relationship between TCPP-Fe organic ligands and different kinds of transition metal ions ( $\text{Cu}^{2+}$ ,  $\text{Ni}^{2+}$ , and  $\text{Fe}^{2+}$ ), the active bulk



**Scheme 2.** Schematic preparation process of the HZ@TCPP-Fe/Cu (where TCPP is tetrakis(4-carboxyphenyl)-porphyrin) heterogeneous catalyst using an “front introduction and rear assembly” encapsulation strategy.

catalysts (TCPP-Fe/Fe bulk, TCPP-Fe/Ni bulk, and TCPP-Fe/Cu bulk) were chosen to illustrate the applicability of the catalytic system. Unexpectedly, the direct mixing of TCPP-Fe and transition metal ions produced a large number of irregularly shaped precipitates, which could not further achieve the purpose of uniform encapsulation (Figures S9–S11, Supporting Information). More deeply, the direct introduction of transition metal ions into ZIF-67@TCPP-Fe (named ZIF-67@TCPP-Fe/Cu, ZIF-67@TCPP-Fe/Ni, and ZIF-67@TCPP-Fe/Fe) could cause the skeleton structure of ZIF-67@TCPP-Fe collapsed due to the ion exchange reaction (Figure S12, Supporting Information).<sup>[22]</sup> In addition, H<sub>4</sub>TPP-Fe organic ligand was chosen to prepare H<sub>4</sub>TPP-Fe/Cu bulk for comparison with the catalytic activity of the above materials (Figure S13, Supporting Information).

The uniformity and integrity of the hollow nanomaterials endow nanocatalysts with unexpected physical and chemical properties.<sup>[23,24]</sup> In our work, a new strategy for preparing hollow HZ nanocage-encapsulated nanoentities under mild conditions was proposed. Powder X-ray diffraction (PXRD) was measured to verify the composition and structural information. The PXRD patterns of all the obtained ZIF-67@TCPP-Fe and ZIF-67@TCPP-Fe/M (M = Cu, Ni, or Fe) materials are consistent with those of bare ZIF-67, confirming their high crystallinity and isostructural nature (Figure 2a).<sup>[25]</sup> For HZ, HZ@TCPP-Fe, and HZ@TCPP-Fe/M, a high-intensity peak appeared at  $2\theta = 10.1^\circ$  related to the (003) facet of the hydrotalcite-like phase (Figure 2b).<sup>[26]</sup> These PXRD results also proved that the hydroxides interlayer spacing of HZ@TCPP-Fe/M was 8.02–9.28 Å. The Fourier transform infrared spectrometer (FT-IR) analysis was explored to verify the construction of these materials (Figure S14, Supporting Information).<sup>[27]</sup> For HZ@TCPP-Fe/M (M = Cu, Ni, or Fe), the morphology of HZ@TCPP-Fe were well maintained after modification (Figure S15, Supporting Information). Specifically, in the thermogravimetric analysis (TGA) profile, the typical weight loss of HZ, HZ@TCPP-Fe and HZ@TCPP-Fe/Cu were attributed to hydroxides decomposition starting at about 210 °C, which differed

with ZIF-67 (500 °C) in temperature (Figure 2c). The chemical composition and oxidation states of HZ@TCPP-Fe and HZ@TCPP-Fe/Cu were studied by high-resolution X-ray photoelectron spectroscopy (XPS) (Figure 2d). The Co 2p spectrum of HZ@TCPP-Fe and HZ@TCPP-Fe/Cu exhibited two distinct peaks centered at 781.12 and 797.27 eV, which were assigned to the 2p<sub>3/2</sub> and 2p<sub>1/2</sub> levels of Co<sup>2+</sup>, respectively. In addition, two broad satellite peaks were located at 785.46 and 802.59 eV (Figure 2e).<sup>[28]</sup> The XPS results revealed that the main oxidation states of Fe in HZ@TCPP-Fe and HZ@TCPP-Fe/Cu materials were +3 (Figure 2f).<sup>[29,30]</sup> The Cu 2p XPS signals appeared at 935.58 and 954.29 eV for Cu 2p<sub>3/2</sub> and Cu 2p<sub>1/2</sub>, respectively (Figure S16, Supporting Information).<sup>[31]</sup> The C 1s peaks of HZ@TCPP-Fe and HZ@TCPP-Fe/Cu can be fitted into C=C (284.43 eV), C=N (285.55 eV), C–O (286.58 eV), and C=O (288.06 eV) (Figure 2g).<sup>[32,33]</sup> The N 1s peaks could be assigned to oxidized N species (NO<sub>3</sub><sup>−</sup>) (406.57 eV) and 2-methylimidazole (399.48 eV) (Figure 2h).<sup>[34]</sup> The peaks of HZ@TCPP-Fe at 531.34 and 533.22 eV were attributed to the O 1s of the C=O and C–OH groups, respectively. However, in HZ@TCPP-Fe/Cu, the peak designated for C=O moved to lower binding energies (531.14 eV), thereby indicating the interaction between the carboxyl group in TCPP-Fe and Cu<sup>2+</sup> (Figure 2i).<sup>[35–37]</sup> Notably, according to Irving–Williams stability series, we noticed that the relative stability of homologous bivalent 3d metal complexes will follow the trend: Cr<sup>2+</sup> < Mn<sup>2+</sup> < Fe<sup>2+</sup> < Co<sup>2+</sup> < Ni<sup>2+</sup> < Cu<sup>2+</sup> > Zn<sup>2+</sup>, regardless of the structure and properties of organic ligands.<sup>[38]</sup> The TCPP-Fe organic ligands were encapsulated in open cavities of ZIFs, and the structure would not be damaged by low-temperature thermal treatment. Then, TCPP-Fe/Cu bimetallic catalytic active sites were constructed by adding Cu<sup>2+</sup> to replace other transition metal ions (such as unquantified Co<sup>2+</sup>) in the carboxyl group of TCPP-Fe.

The ability to prepare a kinetically oriented multivariate hollow nanomaterials with customized layered environment and collaborative behavior provides an unparalleled level of control over the encapsulation and utilization of the “guest.”

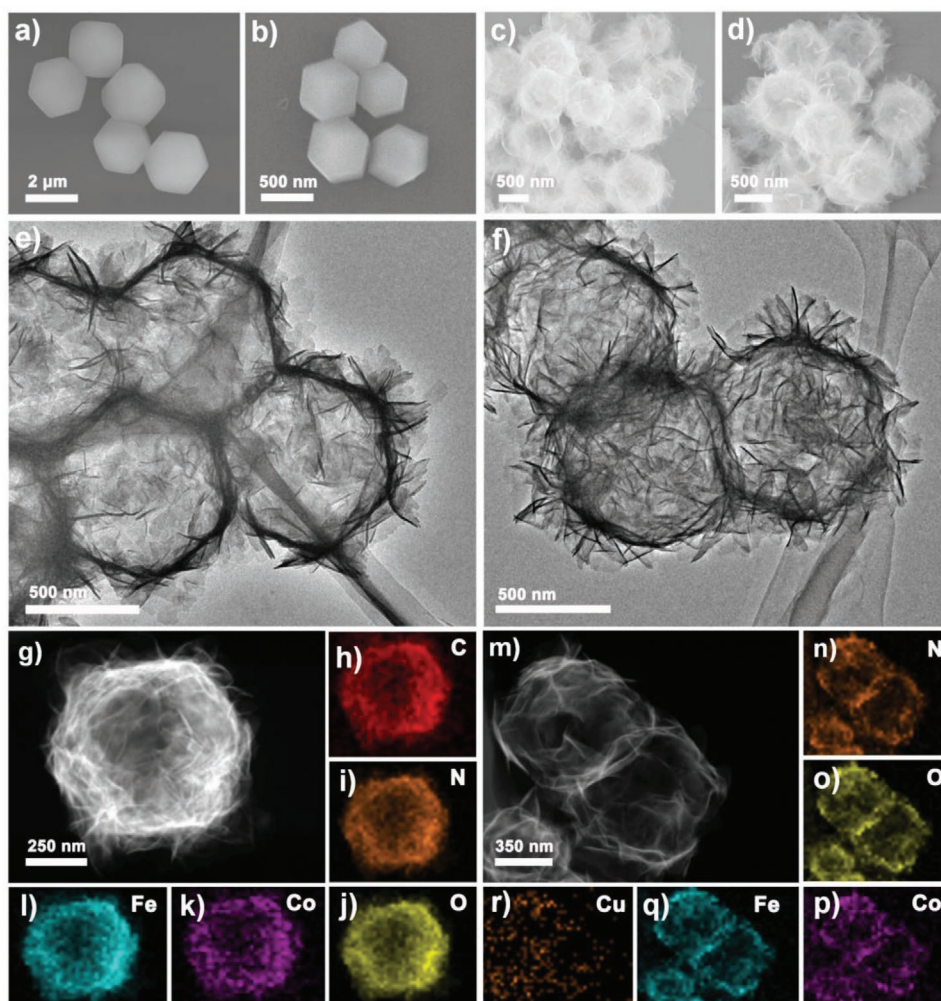


**Figure 1.** Scanning electron microscopy (SEM) images of a) ZIF-67, b) ZIF-67@TCPP-Fe (where TCPP is tetrakis(4-carboxyphenyl)-porphyrin), c) HZ@TCPP-Fe, and d) HZ@TCPP-Fe/Cu. Transmission electron microscopy (TEM) images of e) HZ@TCPP-Fe and f) HZ@TCPP-Fe/Cu. g) The dark-field scanning transmission electron microscopy (STEM) image of HZ@TCPP-Fe. h–l) EDS elemental mapping of C, N, O, Co, and Fe signals for HZ@TCPP-Fe. m) The HAADF-STEM image of HZ@TCPP-Fe/Cu. n–r) EDS elemental mapping of N, O, Co, Fe, and Cu signals for HZ@TCPP-Fe/Cu.

Typically, the *N*-containing imidazole ester on the ZIFs skeleton can provide active uncoordinated nitrogen sites for adsorb “guest” molecules, which makes it more widely used in the field of catalysis than other MOF materials.<sup>[39–41]</sup> To ascertain that the TCPP-Fe “guest” molecules were indeed encapsulated into a porous ZIF-67 carrier, the UV–vis spectrum of ZIF-67 and ZIF-67@TCPP-Fe were measured. ZIF-67@TCPP-Fe displayed a new peak at 411 nm due to the Soret band of TCPP-Fe units (Figure 3a).<sup>[42]</sup> The Raman spectra of ZIF-67, ZIF-67@TCPP-Fe, and ZIF-67@TCPP-Fe/Cu displayed intense bands corresponding to methyl group and imidazole ring vibrations of the ZIFs skeleton. The strong bands at 177, 258, 423, and 686  $\text{cm}^{-1}$  can be attributed to the Zn–N stretching, C–Zn–N bending, and imidazole ring puckering (Figure 3b).<sup>[43]</sup> Unlike rigid inorganic molecular sieves, porous metal–organic frameworks possess good flexibility and are prone to deformation.<sup>[44]</sup> With the introduction of “guest” and postmodification, the wrinkling peaks of the imidazole ring gradually shifted to lower wavenumber, which was caused by the lattice expansion

process.<sup>[45]</sup> The results of time-resolved photoluminescence (TRPL) (Figure 3c; see also Table S2, Supporting Information) confirmed that TCPP-Fe was encapsulated in the open cavities of ZIF-67, which result in a longer carrier lifetime (from 19.78 to 21.28 ns). The average emission lifetime of photoexcited charge for HZ@TCPP-Fe was 21.83 ns, which was longer than that of HZ@TCPP-Fe/Cu (12.03 ns), suggesting that excited-state TCPP-Fe connected with  $\text{Cu}^{2+}$ .<sup>[46]</sup>

In HZ@TCPP-Fe/Cu, the TCPP-Fe/Cu bimetallic sites contained two five-coordinated copper cations that are bridged in a paddle-wheel-type configuration and to which the TCPP-Fe ligands were coordinated in a bidentate bridging fashion.<sup>[47–49]</sup> In  $\text{N}_2$  adsorption and desorption isotherms, compared with ZIF-67, ZIF-67@TCPP-Fe displayed a reduced BET (Brunauer–Emmett–Teller) surface area from 1557 to 1475  $\text{m}^2\text{g}^{-1}$ , due to the mass contributions from TCPP-Fe molecule (Figure 3d). Through the heat treatment process, the hollow layered hydroxide shell structure was gradually formed, and the BET surface area suddenly decreased to 126  $\text{m}^2\text{g}^{-1}$ . For

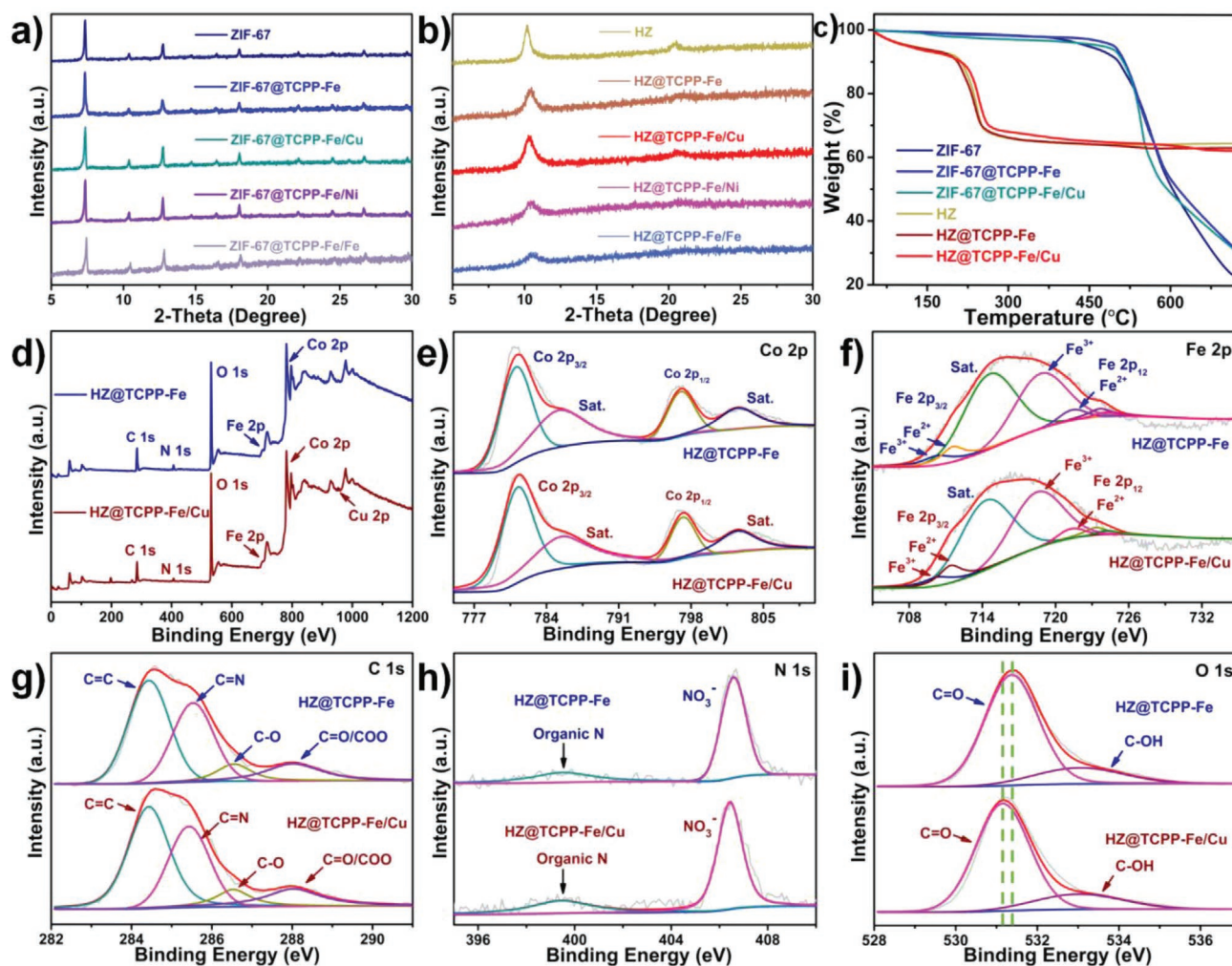


**Figure 2.** a) Powder X-ray diffraction (XRD) patterns of ZIF-67, ZIF-67@TCPP-Fe (where TCPP is tetrakis(4-carboxyphenyl)-porphyrin), ZIF-67@TCPP-Fe/Cu, ZIF-67@TCPP-Fe/Ni, and ZIF-67@TCPP-Fe/Fe. b) Powder XRD patterns of HZ, HZ@TCPP-Fe, HZ@TCPP-Fe/Cu, HZ@TCPP-Fe/Ni, and HZ@TCPP-Fe/Fe. c) The thermogravimetric analysis (TGA) results of ZIF-67, ZIF-67@TCPP-Fe, ZIF-67@TCPP-Fe/Cu, HZ, HZ@TCPP-Fe, and HZ@TCPP-Fe/Cu. d) X-ray photoelectron spectroscopy (XPS) surveys of HZ@TCPP-Fe and HZ@TCPP-Fe/Cu. e–i) The high-resolution Co 2p spectrum (e), Fe 2p spectrum (f), C 1s spectrum (g), N 1s spectrum (h), and O 1s spectrum (i).

HZ@TCPP-Fe and HZ@TCPP-Fe/Cu, the BET surface areas also tended to decrease, owing to the postsynthesis modification process upon the addition of  $\text{Cu}^{2+}$ .

Aromatic azobenzene, as one of the oldest organic compounds, is widely used in the field of chemical industries.<sup>[50–53]</sup> Mitsunobu and co-workers put forward that the combination of diethyl azodicarboxylates and triphenylphosphine causes condensation reactions between alcohols and acids to obtain the corresponding esters.<sup>[54,55]</sup> Previous studies have reported that aromatic azobenzene exhibited effective catalytic ability for Mitsunobu reactions, in which traditional iron(II)phthalocyanine [Fe(Pc)] can be used as an oxidative dehydrogenation catalyst.<sup>[56,57]</sup> However, the aerobic oxidation of Fe(Pc) is difficult to recycle and reuse, has no obvious catalytic selectivity, and often requires a large number of catalysts (10 mol%). Compared with structure-related Fe(Pc), the catalytic performance of TCPP-Fe complexes as the candidates for catalyzing the dehydrogenation of aromatic hydrazides has not been fully studied. For steric

hindrance, smaller aromatic azobenzene may be beneficial to Mitsunobu reaction, so the principle of chemical selectivity is also important. Thus, developing a novel, environmentally friendly, recyclable, and selective catalyst for the dehydrogenation of aromatic hydrazides to aromatic azobenzene is keenly pursued.

In this regard, we focused our studies on the high reactivity and selectivity oxidative dehydrogenation of aromatic hydrazides with different substituents by heterogeneous catalysts under different integration modes (Figure 4a). Being bigger in sizes than ethyl 2-phenylhydrazine-1-carboxylate (**1**) ( $11.5 \times 4.2 \times 1.8 \text{ \AA}^3$ ), the isopropyl 2-phenylhydrazine-1-carboxylate (**2**) ( $11.0 \times 4.2 \times 3.1 \text{ \AA}^3$ ) and *tert*-butyl 2-phenylhydrazine-1-carboxylate (**3**) ( $11.4 \times 4.4 \times 4.4 \text{ \AA}^3$ ) cannot be diffused into HZ@TCPP-Fe/Cu heterogeneous catalyst smoothly and then further oxidized dehydrogenation due to the steric hindrance effect (Figure S17, Supporting Information). Firstly, the catalytic activities toward oxidative dehydrogenation of

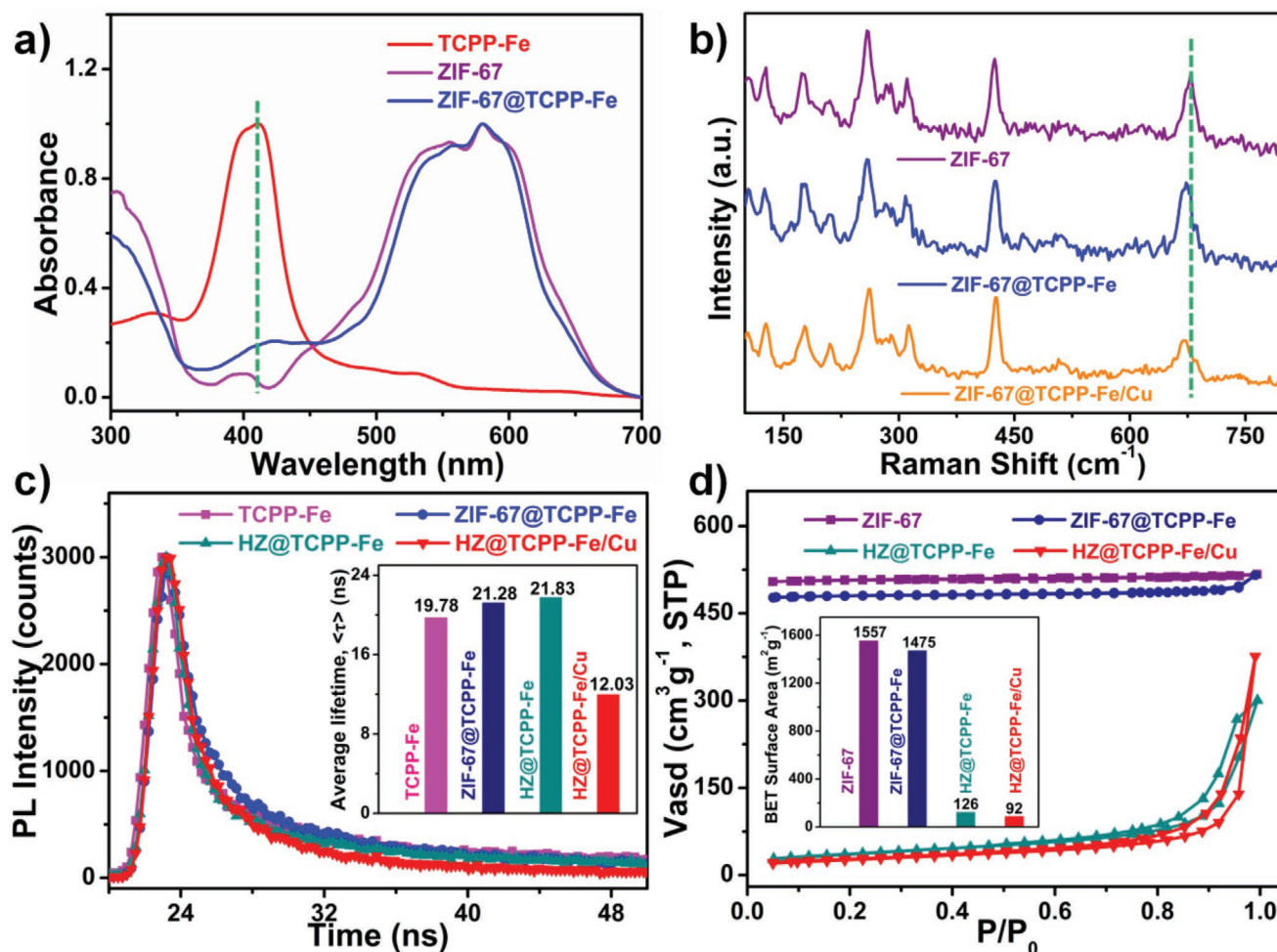


**Figure 3.** a) UV-vis absorption spectra of TCPP-Fe (where TCPP is tetrakis(4-carboxyphenyl)-porphyrin), ZIF-67 (solid samples), and ZIF-67@TCPP-Fe (solid samples). b) Raman spectra of ZIF-67, ZIF-67@TCPP-Fe, and ZIF-67@TCPP-Fe/Cu. c) Time-resolved photoluminescence emission decay spectra of TCPP-Fe, ZIF-67@TCPP-Fe, HZ@TCPP-Fe, and HZ@TCPP-Fe/Cu. d) Nitrogen sorption isotherms for pure ZIF-67, ZIF-67@TCPP-Fe, HZ@TCPP-Fe, and HZ@TCPP-Fe/Cu at 77 K up to 1 bar.

aromatic hydrazides reaction were assessed with 1 mol% active bulk catalysts (TCPP-Fe/Cu bulk, TCPP-Fe/Ni bulk, TCPP-Fe/Fe bulk, and  $H_4$ TPP-Fe/Cu bulk) in  $O_2$ -saturated THF, respectively (Figure 4b). When a mixture of **1** (0.25 mmol) and TCPP-Fe/Cu bulk (1 mol%) in 4 mL THF was exposed to  $O_2$ , ethyl-2-phenyldiazene-1-carboxylate (**4**) was obtained in good yield (>90 %) in 4 h after purification by chromatography. And **2** and **3** also had ideal yields in the same conditions. Furthermore, TCPP-Fe/Fe, TCPP-Fe/Ni, and  $H_4$ TPP-Fe/Cu bulk have good catalytic activity, but slightly inferior to that of TCPP-Fe/Cu. For the above experimental results, we could preliminarily determine that in the structure of the as-prepared active bulk catalysts, porphyrin-Fe as the main component cooperates with the different kinds of transition metal ion, which was indispensable for oxidative dehydrogenation of aromatic hydrazides reaction. When TCPP-Fe or  $H_4$ TPP-Fe exists alone, the catalytic activity was weak (Figure S18, Supporting Information). Besides Fe, Ni, and Cu used in our previous work, the other transition metal atoms including Ag, Mn, and Cr were employed. The SEM images of HZ@TCPP-Fe/Ag, HZ@TCPP-Fe/Mn,

and HZ@TCPP-Fe/Cr were shown in Figure S19 (Supporting Information). From experimental results, compared with HZ@TCPP-Fe/Cu, the above catalysts exhibited weak catalytic activity (Table S3, Entries 1-3, Supporting Information). The combination of metalloporphyrin and electron-deficient metal salt could not only retain the characteristics of metalloporphyrin to activate  $O_2$  and generate free radicals under mild conditions, but also make use of the good adaptability of metal salts toward the reaction conditions, that was, employing metalloporphyrin as inducer and metal salt as promoter to catalyze the oxidation reaction with high activity, which is undoubtedly of great significance. Secondly, to further evaluate the chemoselectivity of catalysts toward primary carbon, the same molar amounts of **1**, **2**, and **3** were used as the reaction substrates, respectively.

Obviously, the hollow HZ@TCPP-Fe/Cu possessed higher catalytic selectivity than the structurally fragmented ZIF-67@TCPP-Fe/Cu, which proved the specific internal voids inside the nanocage successfully controlled the contact between reaction substrates and the catalytic active sites (Figure 4c,d). As the formation of internal voids in HZ@TCPP-Fe/Cu catalyst,

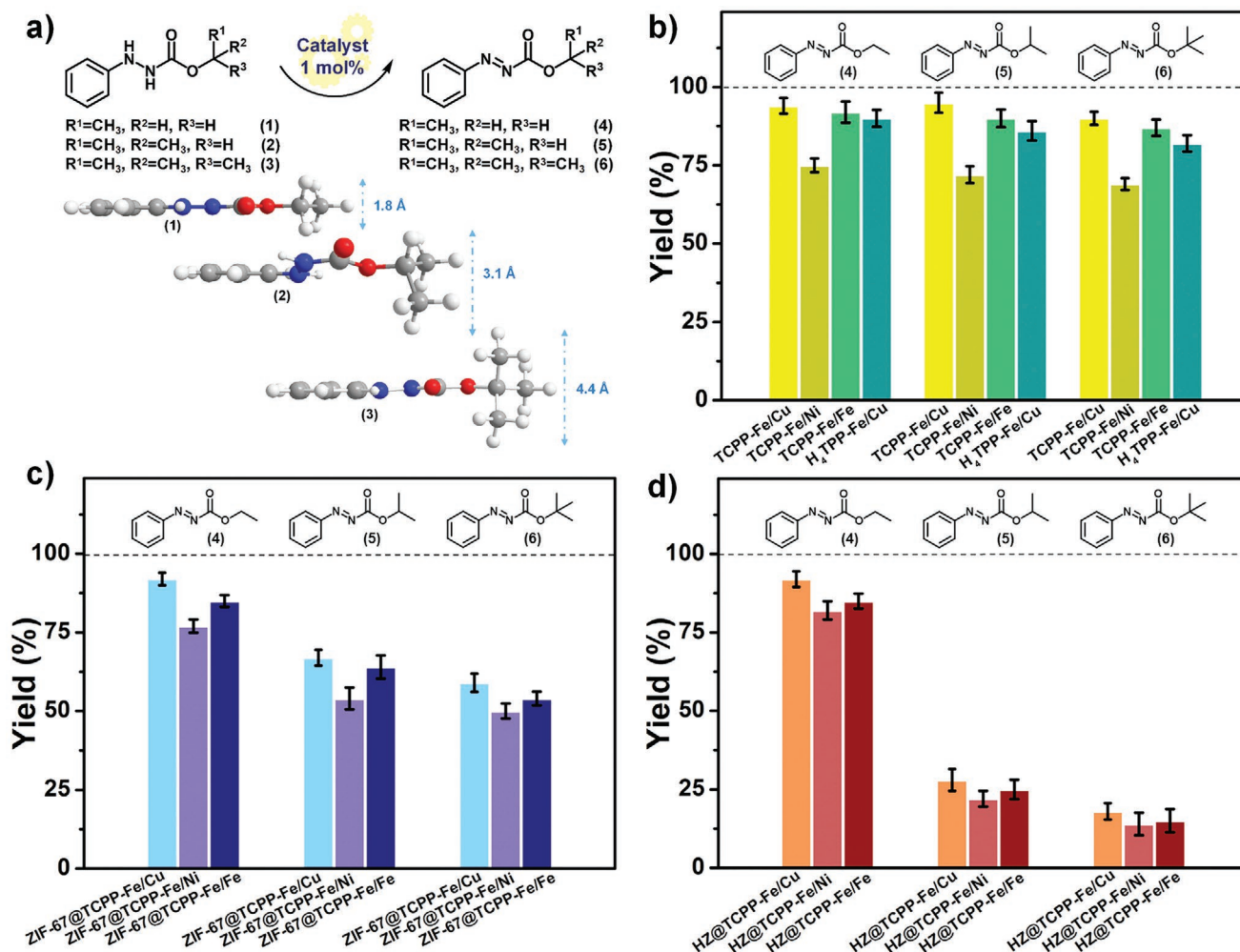


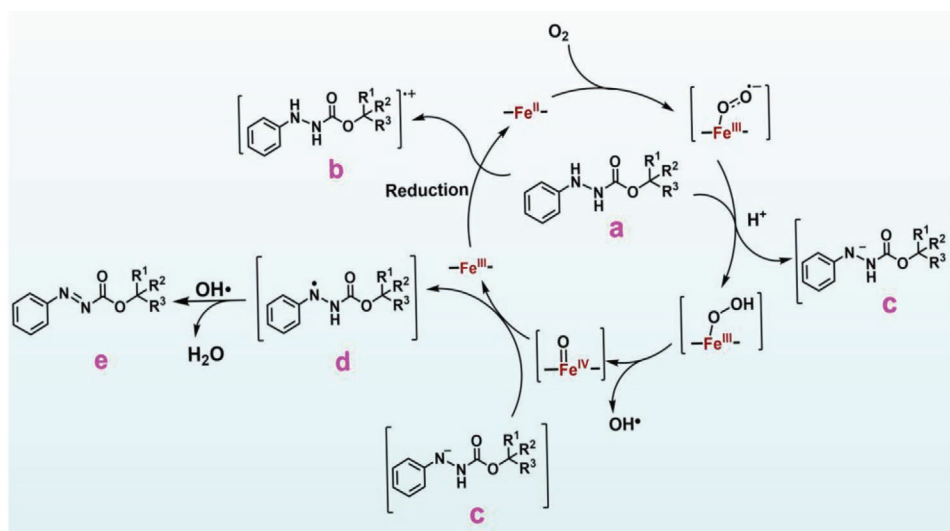
**Figure 4.** a) Concept of a catalytic oxidative dehydrogenation of aromatic hydrazides reactions under different catalysts. b) Catalytic performance of TCPP-Fe/Cu (where TCPP is tetrakis(4-carboxyphenyl)-porphyrin) bulk, TCPP-Fe/Ni bulk, TCPP-Fe/Fe bulk, and H<sub>4</sub>TPP-Fe/Cu bulk toward aromatic hydrazides. c) Catalytic performance of ZIF-67@TCPP-Fe/Cu, ZIF-67@TCPP-Fe/Ni, and ZIF-67@TCPP-Fe/Fe toward aromatic hydrazides. d) Catalytic performance of HZ@TCPP-Fe/Cu, HZ@TCPP-Fe/Ni, and HZ@TCPP-Fe/Fe toward aromatic hydrazides.

the oxidative dehydrogenation of aromatic hydrazides reaction of 2 and 3 were very different from that of 1, the product, 4 (yield > 90%), isopropyl-2-phenyldiazene-1-carboxylate (5) (yield: 24%) and *tert*-butyl-2-phenyldiazene-1-carboxylate (6) (yield: 18%) were generated in low yield in 4 h after purification by chromatography. <sup>1</sup>H NMR analysis of the reactants and products was showed in Figures S20–S25 (Supporting Information). HZ@TCPP-Fe/Cu and ethyl 2-phenylhydrazine-1-carboxylate were chosen as standard catalyst and model substrates to explore the effect of solvent on product yield (Table S4, Supporting Information). We found that, among the various solvents we studied, THF exhibited the best catalytic performance. From experimental results, the HZ@TCPP-Fe/Cu could act as a reaction vessel to promote the oxidative dehydrogenation of aromatic hydrazides reaction, featuring high chemoselectivity toward primary carbons among primary, secondary, and tertiary carbons. And, HZ@TCPP-Fe/Ni and HZ@TCPP-Fe/Fe also had similar catalytic performance. Subsequently, the resulting and highest-performing HZ@TCPP-Fe/Cu was

selected for cyclic and stability tests. Although several cycles of catalysis had been performed, HZ@TCPP-Fe/Cu exhibited satisfactory activity and maintained the morphological and structural integrity (Figure S26, Supporting Information). The PXRD patterns of recyclable HZ@TCPP-Fe/Cu catalyst remained almost unchanged after five cycles (Figure S27, Supporting Information).

For heterogeneous catalysis in hollow nanomaterials, the channel on the thin shell is a necessary factor for the reactants (products) to diffuse into (out of) the catalyst (products). Specifically, the active ingredients can be enriched on the outer surface of the skeleton to form layered hydroxides as the shell of hollow nanomaterials with excellent stability by solvothermal treatment, and then further modified by a “postsynthesis modification” process to obtain a multicomponent heterogeneous catalyst.<sup>[58,59]</sup>

We presented spontaneous phase transformation of ZIF-67@TCPP-Fe from uniform rhombi dodecahedron to HZ@TCPP-Fe under mild solvothermal conditions. The encapsulated



**Scheme 3.** Possible reaction mechanism for oxidative dehydrogenation of aromatic hydrazides catalyzed by HZ@TCPP-Fe/Cu (where TCPP is tetrakis(4-carboxyphenyl)-porphyrin) heterogeneous catalyst.

TCPP-Fe would gradually concentrate on the spherical shell with the formation of the hollow structure, and then coordinated with Cu, increasing the density of local active sites, while avoiding aggregation and inactivation. Specifically, the accessible TCPP-Fe/Cu bimetallic catalytic active sites in the internal voids of HZ@TCPP-Fe/Cu were located on the axial positions porphyrin motifs, which enclosed a confined hydroxides interlayer spacing, imposing more steric effect than TCPP-Fe/Cu bulk or free Fe(Pc).

Molecules of dioxygen at a model Fe(II/III) center are activated to generate oxometal Fe(IV) species, and the generated highly active oxometal Fe(IV) species can act as the active intermediate in many catalytic circulation systems.<sup>[60]</sup> Meanwhile, in the activity of heme-copper oxidase analog which combines Cu and TCPP-Fe, the non-heme metals promote the breaking of the O–O bond.<sup>[61,62]</sup> The higher redox potential and electron density in the *d*-orbital of Cu lead to a weakening of O–O bond, which is the key to the higher activity of oxidase than TCPP-Fe.

On the basis of the literature surveys,<sup>[63–66]</sup> the mechanism of reaction was tentatively proposed (**Scheme 3**). The reaction may be initiated by single-electron transfer between aromatic hydrazides **a** and Fe(III) species to give the cation radical **b**. Meanwhile, the Fe(II) species capture O<sub>2</sub> to generate the superoxide Fe(III) species, and superoxide Fe(III) species extract H<sup>+</sup> from aromatic hydrazides **a** to obtain intermediate **c** and hydroperoxo Fe(III) species. Subsequently, the hydroperoxo Fe(III) species leads to the heterolytic cleavage of the O–O bond, and the formation of a highly active oxometal Fe(IV) species. The oxometal Fe(IV) species get an electron from intermediate **c** to transform to Fe(III) species. The dehydration of intermediate **d** provided the final product **e**.

The promising catalytic activity and selectivity for oxidative dehydrogenation of aromatic hydrazine are ascribed to synergistic effects of bimetal catalytic active site and the limited internal voids in HZ@TCPP-Fe/Cu due to the following reasons: 1) the intermediate tetravalent ferric oxide can be used as an ideal proton acceptor; 2) non-heme Cu can activate

oxygen to accelerate the cleavage of O–O bonds; 3) based on the synergistic effect of TCPP-Fe/Cu bimetallic catalytic active sites, the high reactivity for the target reaction has been established; 4) the TCPP-Fe/Cu bimetallic catalytic active sites are encapsulated in the hydroxide thin shell of the hollow HZ@TCPP-Fe/Cu, which bring additional dimensional selectivity and diffusion differences, thus improving the selectivity of catalytic products.

### 3. Conclusion

In summary, an advanced strategy was developed for the construction of HZ@TCPP-Fe/Cu heterogeneous catalyst through morphology-controlled thermal transformation and rear assemble processes. For HZ@TCPP-Fe/Cu, the catalytic activity of TCPP-Fe was significantly increased when non-heme Cu was involved in assembly. Meanwhile, compared with conventional homogeneous catalysts, a pronounced selectivity enhancement was achieved in oxidative dehydrogenation. Our finding established the potential of hollow nanostructures encapsulated with nanoentities in designing new hybrid inorganic–organic functional materials for heterogeneous catalysis and other fields.

### Supporting Information

Supporting Information is available from the Wiley Online Library or from the author.

### Acknowledgements

D.Z. and P.D. contributed equally to this work. The authors are thankful to the National Natural Science Foundation of China (21575115, 21705117, and 22001193); the Program for Chang Jiang Scholars and Innovative Research Team, Ministry of Education, China (IRT-16R61); the Program of Gansu Provincial Higher Education Research Project (2017-D-01);

Special fund project for the central government to guide local science and technology development (2020); and the Program of Tianjin Science and Technology Major Project and Engineering (19ZXYSY00090). The authors thank Prof. Wenping Hu at Tianjin University for valuable suggestions and help.

## Conflict of Interest

The authors declare no conflict of interest.

## Keywords

encapsulation, heterogeneous catalysts, high selectivity, porphyrin-Fe/Cu complexes, size exclusion

Received: August 2, 2020

Revised: October 3, 2020

Published online:

- [1] S. Huang, X. Kou, J. Shen, G. Chen, G. Ouyang, *Angew. Chem., Int. Ed.* **2020**, *59*, 8786.
- [2] J. Feng, Y. Yin, *Adv. Mater.* **2019**, *31*, 1802349.
- [3] L. Zhang, J. Pan, Y. Long, J. Li, W. Li, S. Song, Z. Shi, H. Zhang, *Small* **2019**, *15*, 1903182.
- [4] L. M. Moreau, C. A. Schurman, S. Kewalramani, M. M. Shahjamali, C. A. Mirkin, M. J. Bedzyk, *J. Am. Chem. Soc.* **2017**, *139*, 12291.
- [5] W. Zhu, Z. Chen, Y. Pan, R. Dai, Y. Wu, Z. Zhuang, D. Wang, Q. Peng, C. Chen, Y. Li, *Adv. Mater.* **2019**, *31*, 1800426.
- [6] Y. Wang, H. Cui, Z. Wei, H. Wang, L. Zhang, C. Su, *Chem. Sci.* **2017**, *8*, 775.
- [7] J. Wu, Y. Yang, *J. Am. Chem. Soc.* **2019**, *141*, 12280.
- [8] D. Zhang, J. Liu, P. Du, Z. Zhang, X. Ning, Y. Deng, D. Yin, J. Chen, Z. Han, X. Lu, *Small* **2020**, *16*, 1905889.
- [9] Y. Wei, N. Yang, K. Huang, J. Wan, F. You, R. Yu, S. Feng, D. Wang, *Adv. Mater.* **2020**, 2002556.
- [10] Y. Wang, D. Adekoya, J. Sun, T. Tang, H. Qiu, L. Xu, S. Zhang, Y. Hou, *Adv. Funct. Mater.* **2019**, *29*, 1807485.
- [11] W. Wu, L. Yu, Y. Pu, H. Yao, Y. Chen, J. Shi, *Adv. Mater.* **2020**, *32*, 2000542.
- [12] Q. Wu, L. Yang, X. Wang, Z. Hu, *Adv. Mater.* **2020**, *32*, 1904177.
- [13] J. Zhang, L. Yu, Y. Chen, X. Lu, S. Gao, X. Lou, *Adv. Mater.* **2020**, *32*, 1906432.
- [14] Y. Deng, Z. Zhang, P. Du, X. Ning, Y. Wang, D. Zhang, J. Liu, S. Zhang, X. Lu, *Angew. Chem., Int. Ed.* **2020**, *59*, 6082.
- [15] S. Dutta, N. Kumari, S. Dubbu, S. W. Jang, A. Kumar, H. Ohtsu, J. Kim, S. H. Cho, M. Kawano, I. S. Lee, *Angew. Chem., Int. Ed.* **2020**, *59*, 3416.
- [16] J. Noel, N. Kostopoulos, C. Achaibou, C. Fave, E. Anxolabéhère-Mallart, F. Kanoufi, *Angew. Chem., Int. Ed.* **2020**, *59*, 16376.
- [17] R. D. Mukhopadhyay, Y. Kim, J. Koo, K. Kim, *Acc. Chem. Res.* **2018**, *51*, 2730.
- [18] X. Ning, B. Lu, Z. Zhang, P. Du, H. Ren, D. Shan, J. Chen, Y. Gao, X. Lu, *Angew. Chem., Int. Ed.* **2019**, *58*, 16800.
- [19] R. A. Ghiladi, R. M. Kretzer, I. Guzei, A. L. Rheingold, Y. M. Neuhold, K. R. Hatwell, A. D. Zuberbühler, K. D. Karlin, *Inorg. Chem.* **2001**, *40*, 5754.
- [20] S. M. Adam, G. B. Wijeratne, P. J. Rogler, D. E. Diaz, D. A. Quist, J. J. Liu, K. D. Karlin, *Chem. Rev.* **2018**, *118*, 10840.
- [21] Q. Lu, J. Song, P. Wu, C. Li, W. Thiel, *ACS Catal.* **2019**, *9*, 4892.
- [22] S. H. Lee, H. Y. Seo, Y. S. Yeom, J. E. Kim, H. An, J. Lee, H. Jeong, K. Baek, K. Y. Cho, H. G. Yoon, *Polymer* **2018**, *150*, 159.
- [23] H. Song, Y. You, J. Geng, Z. Gu, J. Zou, C. Yu, *Adv. Mater.* **2019**, *31*, 1801564.
- [24] P. Qiu, B. Ma, C. Hung, W. Li, D. Zhao, *Acc. Chem. Res.* **2019**, *52*, 2928.
- [25] X. Deng, L. Yang, H. Huang, Y. Yang, S. Feng, M. Zeng, Q. Li, D. Xu, *Small* **2019**, *15*, 1902287.
- [26] T. Li, G. Li, L. Li, L. Liu, Y. Xu, H. Ding, T. Zhang, *ACS Appl. Mater. Interfaces* **2016**, *8*, 2562.
- [27] R. R. Kuruppathparambil, T. Jose, R. Babu, G. Hwanga, A. C. Kathalikkattil, D. Kim, D. Park, *Appl. Catal., B* **2016**, *182*, 562.
- [28] S. Choi, O. h. M, *Angew. Chem., Int. Ed.* **2019**, *58*, 866.
- [29] C. Hou, L. Zou, Q. Xu, *Adv. Mater.* **2019**, *31*, 1904689.
- [30] Y. Wang, C. Xie, Z. Zhang, D. Liu, R. Chen, S. Wang, *Adv. Funct. Mater.* **2018**, *28*, 1703363.
- [31] Z. Li, J. Chu, D. Meng, Y. Wen, X. Xing, H. Miao, M. Hu, C. Yu, Z. Wei, Y. Yang, Y. Li, *ACS Catal.* **2019**, *9*, 8659.
- [32] R. Jiang, L. Li, T. Sheng, G. Hu, Y. Chen, L. Wang, *J. Am. Chem. Soc.* **2018**, *140*, 11594.
- [33] S. Zhang, B. Guan, X. Lou, *Small* **2019**, *15*, 1805324.
- [34] G. Yilmaz, K. M. Yam, C. Zhang, H. Fan, G. Ho, *Adv. Mater.* **2017**, *29*, 1606814.
- [35] Y. Wang, M. Zhao, J. Ping, B. Chen, X. Cao, Y. Huang, C. Tan, Q. Ma, S. Wu, Y. Yu, Q. Lu, J. Chen, W. Zhao, Y. Ying, H. Zhang, *Adv. Mater.* **2016**, *28*, 4149.
- [36] L. An, J. Feng, Y. Zhang, Y. Zhao, R. Si, G. Wang, F. Cheng, P. Xi, S. Sun, *Nano Energy* **2019**, *57*, 644.
- [37] X. Jin, Y. Duan, D. Liu, X. Feng, W. Li, Z. Zhang, Y. Zhang, *ACS Appl. Nano Mater.* **2019**, *2*, 5769.
- [38] M. S. Kandanapitisye, F. J. Wang, B. Valley, C. Gunathilake, M. Jaroniec, S. D. Huang, *Inorg. Chem.* **2015**, *54*, 1212.
- [39] X. Qiao, B. Su, C. Liu, Q. Song, D. Luo, G. Mo, T. Wang, *Adv. Mater.* **2018**, *30*, 1702275.
- [40] P. Cui, Y. Ma, H. Li, B. Zhao, J. Li, P. Cheng, P. B. Balbuena, H. Zhou, *J. Am. Chem. Soc.* **2012**, *134*, 18892.
- [41] T. Wei, S. Wu, Y. Huang, W. Lo, B. P. Williams, S. Chen, H. Yang, Y. Hsu, Z. Lin, X. Chen, P. Kuo, L. Chou, C. Tsung, F. Shieh, *Nat. Commun.* **2019**, *10*, 5002.
- [42] K. Yuan, T. Song, D. Wang, X. Zhang, X. Gao, Y. Zou, H. Dong, Z. Tang, W. Hu, *Angew. Chem., Int. Ed.* **2018**, *57*, 5708.
- [43] G. Kumari, K. Jayaramulu, T. K. Maji, C. Narayana, *J. Phys. Chem. A* **2013**, *117*, 11006.
- [44] K. W. Chapman, G. J. Halder, P. J. Chupas, *J. Am. Chem. Soc.* **2009**, *131*, 17546.
- [45] E. Sediva, T. Defferriere, N. H. Perry, H. L. Tuller, J. L. M. Rupp, *Adv. Mater.* **2019**, *31*, 1902493.
- [46] J. Wang, H. Chen, F. Ru, Z. Zhang, X. Mao, D. Shan, J. Chen, X. Lu, *Chem. - Eur. J.* **2018**, *24*, 3499.
- [47] G. Zhan, L. Fan, F. Zhao, Z. Huang, B. Chen, X. Yang, S. Zhou, *Adv. Funct. Mater.* **2019**, *29*, 1806720.
- [48] D. Song, J. Bae, H. Ji, M. Kim, Y. Bae, K. Park, D. Moon, N. C. Jeong, *J. Am. Chem. Soc.* **2019**, *141*, 7853.
- [49] M. Saraf, R. Rajak, S. M. Mobin, *J. Mater. Chem. A* **2016**, *4*, 16432.
- [50] P. T. Wong, S. K. Choi, *Chem. Rev.* **2015**, *115*, 3388.
- [51] D. Hirose, M. Gazvoda, J. Košmrlj, T. Taniguchi, *Chem. Sci.* **2016**, *7*, 5148.
- [52] X. Wang, X. Wang, C. Xia, L. Wu, *Green Chem.* **2019**, *21*, 4189.
- [53] R. H. Beddoe, K. G. Andrews, V. Magné, J. D. Cuthbertson, J. Saska, A. L. Shannon-Little, S. E. Shanahan, H. F. Sneddon, R. M. Denton, *Science* **2019**, *365*, 910.
- [54] O. Mitsunobu, M. Yamada, T. Mukaiyama, *Bull. Chem. Soc. Jpn.* **1967**, *40*, 935.
- [55] O. Mitsunobu, M. T. Yamada, *Bull. Chem. Soc. Jpn.* **1967**, *40*, 2380.
- [56] A. B. Sorokin, *Chem. Rev.* **2013**, *113*, 8152.
- [57] K. Gopalaiyah, *Chem. Rev.* **2013**, *113*, 3248.
- [58] C. Jiao, Z. Wang, X. Zhao, H. Wang, J. Wang, R. Yu, D. Wang, *Angew. Chem., Int. Ed.* **2019**, *58*, 996.
- [59] B. Zhang, Z. Qi, Z. Wu, Y. Lui, T. Kim, X. Tang, L. Zhou, W. Huang, S. Hu, *ACS Energy Lett.* **2019**, *4*, 328.

- [60] D. Kass, T. Corona, K. Warm, B. Braun-Cula, U. Kuhlmann, S. M. E. Bill, M. Swart, H. Dau, M. Haumann, P. Hildebrandt, K. Ray, *J. Am. Chem. Soc.* **2020**, *142*, 5924.
- [61] A. Bhagi-Damodaran<sup>1</sup>, M. A. Michael, Q. Zhu, J. Reed, B. A. Sandoval, E. N. Mirts, S. Chakraborty, P. Moënne-Loccoz, Y. Zhang, Y. Lu, *Nat. Chem.* **2019**, *11*, 622.
- [62] A. W. Schaefer, M. T. Kieber-Emmons, S. M. Adam, K. D. Karlin, E. I. Solomon, *J. Am. Chem. Soc.* **2017**, *139*, 7958.
- [63] T. Hashimoto, D. Hirose, T. Taniguchi, *Adv. Synth. Catal.* **2015**, *357*, 3346.
- [64] T. Taniguchi, Y. Sugiura, H. Zaimoku, H. Ishibashi, *Angew. Chem., Int. Ed.* **2010**, *49*, 10154.
- [65] X. Huang, J. T. Groves, *Chem. Rev.* **2018**, *118*, 2491.
- [66] M. L. Pegis, D. J. Martin, C. F. Wise, A. C. Brezny, S. I. Johnson, L. E. Johnson, N. Kumar, S. Raugei, J. M. Mayer, *J. Am. Chem. Soc.* **2019**, *141*, 8315.